



Technical Note

74

**SCATTERING OF COBALT-60 GAMMA
RADIATION IN AIR DUCTS**



**U. S. DEPARTMENT OF COMMERCE
NATIONAL BUREAU OF STANDARDS**

THE NATIONAL BUREAU OF STANDARDS

Functions and Activities

The functions of the National Bureau of Standards are set forth in the Act of Congress, March 3, 1901, as amended by Congress in Public Law 619, 1950. These include the development and maintenance of the national standards of measurement and the provision of means and methods for making measurements consistent with these standards; the determination of physical constants and properties of materials, the development of methods and instruments for testing materials, devices, and structures; advisory services to government agencies on scientific and technical problems; invention and development of devices to serve special needs of the Government; and the development of standard practices, codes, and specifications. The work includes basic and applied research, development, engineering, instrumentation, testing, evaluation, calibration services, and various consultation and information services. Research projects are also performed for other governmental agencies when the work relates to and supplements the basic program of the Bureau in which the Bureau's unique competence is required. The scope of activities is suggested by the listing of divisions and sections on the inside of the back cover.

Publications

The results of the Bureau's work take the form of either actual equipment and devices or published papers. These papers appear either in the Bureau's own series of publications or in the journals of professional and scientific societies. The Bureau itself publishes three periodicals available from the Government Printing Office: The Journal of Research, published in four separate sections, presents complete scientific and technical papers; the Technical News Bulletin presents summary and preliminary reports on work in progress; and Basic Radio Propagation Prediction provides data for determining the best frequencies to use for radio communications throughout the world. There are also five series of nonperiodical publications: Monographs, Applied Mathematics Series, Handbooks, Miscellaneous Publications, and Technical Notes.

Information on the Bureau's publications can be found in NBS Circular 500, *Publications of the National Bureau of Standards* (\$1.25) and its Supplement (\$1.50), available from the Superintendent of Documents, Government Printing Office, Washington 25, D.C.

NATIONAL BUREAU OF STANDARDS

Technical Note

74

OCTOBER 1960

SCATTERING OF COBALT-60 GAMMA RADIATION IN AIR DUCTS

Charles Eisenhauer



The work described in this Technical Note was sponsored by the Office of Civil and Defense Mobilization, the Bureau of Yards and Docks, Department of the Navy, and the Defense Atomic Support Agency, Department of Defense.

NBS Technical Notes are designed to supplement the Bureau's regular publications program. They provide a means for making available scientific data that are of transient or limited interest. Technical Notes may be listed or referred to in the open literature. They are for sale by the Office of Technical Services, U. S. Department of Commerce, Washington 25, D. C.

DISTRIBUTED BY
UNITED STATES DEPARTMENT OF COMMERCE
OFFICE OF TECHNICAL SERVICES
WASHINGTON 25, D. C.

Price 75 cents

Scattering of Cobalt-60 Gamma Radiation in Air Ducts

Charles Eisenhauer

The exposure dose rates due to Cobalt-60 gamma radiation scattered in small air ducts in concrete has been measured for ducts with one and two right angle bends. The inside corner of a right angle bend has been found to be an important source of scattered radiation. Results are analyzed in terms of solid angle relationships and attempts are made to extrapolate experimental results to other duct configurations.

1. Introduction

Although the scattering of nuclear radiation in air ducts within a shield is a common problem, the tendency has been to treat only specific duct configurations. For example, designers of reactor shields have been concerned with the penetration of radiation from reactors through beam ports and other relatively small ducts in the reactor's biological shield. On the other hand, designers of radiological shelters have been concerned with the penetration of radiation from nuclear weapons through the much larger entranceways associated with shelters. More recently, with the advent of high intensity gamma ray sources, calculation of the scattering of gamma radiation in passageways leading from the source chamber to the surrounding environment has become an important problem. The proper design of ducts over this large range of configurations requires a more detailed knowledge of the scattering processes in a duct. Accordingly, an experimental investigation was undertaken to study the scattering of Cobalt-60 gamma radiation in air ducts in concrete. Ducts with one and two right angle bends were studied. The investigation was restricted to ducts with a uniform cross sectional area.

2. Experimental Arrangement

Measurements were made on small (less than 1 square foot area) air ducts in a concrete medium. A typical duct configuration with the overhead shielding blocks removed is shown in figure 1. The duct shielding consists of solid concrete blocks with an average density of 124 pounds per cubic foot. In all measurements, the distance from the source to the geometrical center of the first junction was 100 centimeters. The experiment was run for three different duct cross sections; namely, 19.2 cm x 19.2 cm, 28.2 cm x 28.2 cm, and 19.2 cm x 28.2 cm. The source used in this experiment was a collimated Cobalt-60 source of 1 curie nominal strength replaced later by one of 4 curies. When a lead plug was removed from the lead source-container the radiation from the gamma source was emitted within a cone of half angle, α , such that $\tan \alpha = 0.3$. (See figure 2.) Under these conditions radiation strikes the walls of the 28.2 cm duct, for example, about half-way down the duct and therefore the junction in all cases is well illuminated by the source radiation.

The detectors used in this experiment are shown in figure 3. The two chambers on the right are the non-self-reading Victoreen Model 362 pocket ionization chambers which are used very frequently in personnel protection. These chambers are useful in the dose range of 20 to 200 mr. For low intensity levels we used the larger cylindrical chamber 3 inches high and 2 inches in diameter, shown on the left. The latter is useful in the range of 1 to 10 mr. All readings in this experiment were made on the Victoreen minometer type of electrometer shown in the figure.

All measurements were taken with the axis of the chamber perpendicular to the plane formed by the axes of the two legs of the duct. The chambers were supported in the aluminum holder shown in figure 3. The center of the chamber was taken as the effective detector position.

Measurements by Day [1] indicate that the energy response of the pocket ionization chambers is uniform down to about 250 kev. More recent measurements by Sanders, Auxier, and Cheka [2] confirm this and also indicate that the directional response of the pocket ionization chambers is isotropic for radiation impinging at angles from 30° to 90° with the axis of the chamber. The response decreases from a response of unity at 30° to a response of $1/2$ at 0° (radiation parallel to the axis). They found, furthermore, that the addition of 40 mils of tin on the cap-end of the chamber improves the energy response making it uniform down to about 50 kev and at the same time makes the angular response of the detector more nearly isotropic for low energy radiation.

The tin absorber was used in this experiment to check for spuriously high readings due to the presence of low energy radiation. It is shown in place on the middle chamber in figure 3. Readings taken with the 200 mr chambers at $D = 20$ cm and $D = 50$ cm indicated a difference of less than 5% with and without the tin absorber. This seems to indicate that there is no significant component of low energy radiation, but rather that the bulk of the radiation present is concentrated about an energy of ~ 350 kev, corresponding to a single scatter of 90° .

Measurements by the Army Chemical Center [3] on the 10 mr dosimeters indicate that they are even more isotropic in response than the pocket ionization chambers. Although no energy response measurements have been taken on the 10 mr chambers, dose rates measured at several points both with the 200 mr chambers and the 10 mr chambers show good agreement.

3. Results

3.1 Single Bend

The segment of the duct between the source and the first bend will be referred to as the first leg of the duct. The attenuation in the first leg of the duct is not discussed here because it is so sensitive to the angular distribution of the source radiation. For example, if the source were a parallel beam then there would be no attenuation at all in the primary leg since the dose rate at the entrance of the first leg and at the junction would be the same. On the other hand, if the flux at the entrance to the first leg is an isotropic flux then the dose rate from unscattered radiation at any point along the primary leg of the duct will be inversely proportional to the square of the distance from the source. It is assumed, therefore, in this paper that the dose rate at the first junction of the duct can be either measured or calculated for the particular source geometry involved.

The measured exposure dose rates along the central axis of the second leg of the duct are shown in figure 4 for three different sized ducts. The distance D is measured from the geometrical center of the duct junction to the effective detector position. The first trend that became apparent in this experiment was that the dose rate in the second leg of the duct varied more nearly as $\frac{1}{D^3}$ rather than as $\frac{1}{D^2}$.

(This is shown in figure 5.) A $1/D^2$ variation can be interpreted as a simple solid angle relationship since the solid angle, Ω , approaches

$\frac{HW}{D^2}$ for D much larger than the height H and the width W of the duct.

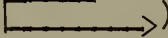
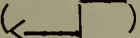
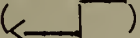
The solid angle would be that subtended at the detector by a hypothetical plane radiator of area HW located at the center of the junction, normal to the axis of the second leg of the duct.

3.2 Effect of Corner

It is important to know which wall surfaces of the junction are the most important secondary sources of scattered radiation. If we assume that the two walls forming the outside corner of the junction are the most important secondary sources, and that they contribute about equally, then setting back one of the walls to form a radiation trap should reduce the dose rates in the second leg by about 50%. Setting back one wall about a mean free path, however, produced only about a 15% decrease in dose rate. Further investigation showed that this was because scattering in the inside corner of the junction accounted for about half of the dose rate and was therefore unaffected by setting back the walls of the junction. This was a rather unexpected result. The concrete of the inside corner of the junction and the rear wall of the second leg (the wall nearest the source) was replaced with Pb and the measurements were repeated. Results are shown in figure 6. Tests showed that most of the difference was due to the Pb which was within 6 inches of the corner. Since the lead and concrete blocks were not co-modular, the duct geometry with the lead corner was somewhat distorted and therefore different from the original geometry. The error due to this distortion is not expected to be greater than about 20%. Nevertheless, the measurements with Pb should be considered only as a qualitative estimate of the effect of the corner contribution.

The relative contribution from the corner should decrease as the duct size increases. This can be seen from the following argument. The dose rate at a fixed distance from the junction due to the corner scatter will be approximately proportional to the duct height ($\sim H$), while that due to reflection from the junction walls will vary as the area of the duct ($\sim H \times W$). Therefore, for large ducts ($\mu_0 W/2 \gg 1$) the ratio of the corner contribution to the reflected contribution approaches zero. Here μ_0 is the mean free path in the surrounding medium.

3.3. Double Turn

The dose rate in a duct having two right-angle turns was also investigated. The dose rates in the third leg are presented in figure 7 as ratios of the measured dose rate R , to the dose rate R_0 at the center of the second junction. The ratios were measured for the case of two right angle turns of the same sense () and two turns of the opposite sense (). Shown for comparison is the dose rate in the second leg relative to the dose rate at the first junction plotted against distance from the first junction. It is seen that the behavior is very different both in magnitude and in rate of decrease with distance. The ratios for distances of less than 14.1 cm correspond to locations which are within the junction. They therefore follow the trend of the dose rates in the leg preceding the junction. Thus, the dose rate ratio, in the case of the () duct, increases at first, due to the distribution in the second leg, and then decreases when the detector is located beyond the junction in the third leg of the duct.

4. Discussion

We now look for an analytical expression with which we can fit the experimental data. We know that each wall of the junction including the inside corner, contributes to the dose rate in the second leg. One approach is to calculate the contribution from each wall and the corner separately. This approach is being tried by J. C. LeDoux [4] at the Naval Civil Engineering Laboratory using the albedo data generated by Berger and Raso [5]. We prefer, however, to look for a composite expression which includes the corner contribution and thus describes the total radiation received at the detector. This expression should be valid for large and small ducts alike.

In the past it has been generally assumed that the dose rate should be proportional to the solid angle subtended at the detector by the junction. The ratio of the dose rate R at the detector to the dose rate R_0 at the center of the junction can then be written as

$$R/R_0 = k\omega$$

where k depends on the characteristics of the junction but not on the detector position. In order to calculate the solid angle ω , the junction must be replaced by a hypothetical radiating area at a distance D from the detector. It has never been clear, however, how this distance should be defined. In our experiment we find that if we measured distance from the center of the junction, the dose rate

varies as $\frac{1}{D^3}$. We now ask if there is any way of defining the distance such that the dose rate will vary more closely with $\frac{1}{D^2}$ and

thus be proportional to solid angle. After investigation we found

that we could do this by defining a new distance D' which is equal to

$$\left(D - \frac{W}{2} - \frac{1}{\mu}\right).$$

The choice of such a definition can be justified by reference to figure 8. For a large duct ($W \gg 1/\mu$) the distance D' is effectively the distance from the exit face of the junction. For a small duct, however, D' is the distance from a plane located one mean free path into the second leg. Thus the inside corner is recognized as an integral part of the junction.

The expression for the solid angle fraction (see reference 6),

$\omega = \frac{\Omega}{2\pi}$, subtended by a rectangle is

$$\omega = \frac{2}{\pi} \tan^{-1} \frac{\varepsilon}{\eta \sqrt{\eta^2 + \varepsilon^2 + 1}}$$

where ε and η are two eccentricity parameters. Their values in terms of the parameters of this report are

$$\varepsilon = W/H \quad \text{and}$$

$$\eta = 2 D/H$$

We have calculated ω as a function of D' , substituting D' for D in the formula for η .

A plot of the measured ratio $\frac{R}{R_0}$ against ω is shown in figure 9 for a duct with one right-angle bend. From the observed linear relationship we may say that $\frac{R}{R_0}$ is equal to $k_1 \times \omega$ where $k_1 = 0.095 \pm .005$. The subscript 1 on k refers to the first junction. Furthermore, if we compare this expression with data taken on large ducts at Brookhaven National Laboratory [7] we find that $\frac{R}{R_0} = k'_1 \omega$, where k'_1 differs from k_1 by only 20%. The data taken at Brookhaven are also shown in figure 9. It should be noted that this behavior applies only to point sources where the value of the source-to-junction distance is large compared to the width of the first leg. There is some evidence from Brookhaven that the behavior of the dose rate in the second duct will change if the source-junction distance is reduced significantly.

We now ask how the constant k_1 might vary for other kinds of ducts. In this discussion we take the approach that the radiation reaching the detector is singly scattered radiation from scattering centers in the walls of the junction. The energy scattered at angle θ is then equal to the product of the average fraction $f(E_0)$ of energy retained by the scattered photon in a collision and the fraction $p(\cos\theta)$ of the scattered energy radiated at an angle θ :

$$k_1 = f(E_0)p(\cos\theta)$$

As an approximation we assume that the angular distribution of scattered energy assumes the angular distribution of the energy of singly-scattered Compton photons

$$p(\cos\theta) \approx K(\theta) = 2\pi E(\cos\theta) \frac{d\sigma}{d\Omega}(\cos\theta) \left\{ \int_{4\pi} E(\cos\theta') \frac{d\sigma}{d\Omega}(\cos\theta') d\Omega' \right\}^{-1}.$$

where $E(\cos\theta)$ is the energy of singly scattered Compton radiation, $\frac{d\sigma(\cos\theta)}{d\Omega}$ is the Klein-Nishina differential cross section for a

scattering angle θ , and the constant 2π is a conversion from solid angle Ω , to solid angle fraction ω . $K(\theta)$ is shown in figure 10 for $E_0 = 1.2$ Mev. We then expect that in ducts with bends of angles other than 90° the intensity as a function of the duct angle should follow this relationship. The horizontal line at $p(\cos\theta) = 1/2$ gives the result for an isotropic angular distribution. Also, shown for comparison is the $(\sin\theta)^{-1}$ trend which has been assumed in the past [8] as the dependence on the angle of the bend at the duct. It is seen that the Klein-Nishina formula predicts a more severe variation with angle. The value for 90° is 0.17. The average fraction, $f(E_0)$, retained by the photon has been calculated by Nelms. [9] For Cobalt-60 the value is $f = 0.53$. Thus, the value of k predicted from these considerations is

$$k_1 = (0.17)(0.53) = 0.090$$

in close agreement with the value obtained from these measurements.

Let us now look at the dose rate variation in the third leg of the duct. The dose rate ratios for the two types of right angle bends are shown in figure 11. The solid angle ω is now computed in terms of a distance D'' given by

$$D'' = D - \frac{W}{2} - \frac{1}{\mu'}$$

where $\frac{1}{\mu'}$ is the mean free path corresponding to the average energy

(~ 350 kev) of radiation in the second leg. Although the dose rate ratio in the third leg is approximately proportional to ω , the absolute value is much greater than that in the second leg. The dose rate ratios are given by

$$R/R_0 = 0.8\omega \quad \left(\leftarrow \overline{\quad} \right) \text{ case}$$

and

$$R/R_0 = 0.5\omega \quad \left(\overline{\quad} \rightarrow \right) \text{ case}$$

The difference in magnitude between these two cases for values of ω near unity is a consequence of the dose rate distribution in the second leg. Although parallel lines have been drawn through the two sets of data, it is not clear whether or not the two sets of data would approach each other for very small values of ω .

The second junction has an apparent albedo which is five to eight times greater than that of the first junction. Care must be taken, however, in the interpretation of these numbers because the reference dose rate varies rather widely over the dimensions of the second junction. For example, if the dose rates were related to the measured dose rate R_1 at the entrance of the junction minus one mean free path instead of R_0 at the center of the junction, the new values of k_2 would be

$$k_2' = k_2 \frac{R_0}{R_1} = 0.8 \times \frac{3.71}{8.5} = 0.35 \left(\leftarrow \overline{\quad} \right) \text{ case}$$

$$k_2' = k_2 \frac{R_0}{R_1} = 0.5 \times \frac{3.71}{8.5} = 0.22 \left(\overline{\quad} \rightarrow \right) \text{ case}$$

Revising the value of k_1 in a similar manner would yield

$$k_1' = k_1 \frac{R_0}{R_1} = 0.095 \times \frac{1050}{1712} = 0.058$$

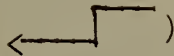
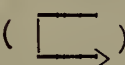
and the albedo for the second junction would now be four to six times greater than that of the first junction. Thus the ratio of the apparent albedo of the first and second junctions is quite sensitive to the manner in which the albedo is defined.

Following the reasoning used in the last section for predicting k we calculate another $K(\theta)$ distribution corresponding to a source energy of 350 kev and find that the value of $K(\theta = 90^\circ)$ is 0.27. The value from reference 9 for the fraction of energy retained by a photon of energy $E = 350$ kev is 0.71. The predicted value of k_2 is

$$k_2 = (0.27)(0.71) = 0.19$$

which is closer to the empirical value obtained when defined in terms of the dose rate at the entrance to the junction rather than at the center. A comparison of the predicted values of k and the experimental values obtained for each definition is shown in table 1.

Table 1

	Experimental		Predicted
	$k = \frac{R}{R_0} \times \frac{1}{\omega}$	$k' = \frac{R}{R_1} \times \frac{1}{\omega}$	$k = f(E_0)p(\cos\theta=0)$
First bend	0.095	0.058	0.090
Second bend ()	.80	.35	.19
()	.50	.22	.19

Although the predicted value of k for the second junction is more consistent with the experimental values of k' , the disagreement is severe enough to suggest further study. The predicted value of k for the first junction however, is in good agreement with the experimental value of $k = 0.095$.

5. Acknowledgment

The author wishes to thank Dr. L. V. Spencer for suggesting this experiment and for many helpful discussions. Many thanks also to R. Bach, O. H. Hill, and Mrs. S. Ripps for technical assistance in preparing this report.

6. References

- [1] F. H. Day, X-ray calibration of radiation survey meters, pocket chambers, and dosimeters, NBS Circular 507, (July 1951).
- [2] F. W. Sanders, J. A. Auxier, and J. S. Cheka, A simple method of minimizing the energy dependence of pocket ionization chambers, Health Physics 2, No. 3, (Feb. 1960).
- [3] R. Rexroad (private communication).
- [4] J. C. LeDoux (private communication).
- [5] M. J. Berger and D. J. Raso, Monte Carlo calculations of gamma-ray backscattering, Radiation Research 12, 1, (Jan. 1960).
- [6] L. V. Spencer, Structure shielding against fallout radiation from nuclear weapons, (to be published by Office of Civil and Defense Mobilization, Washington, D.C.).
- [7] F. Rizzo (private communication).
- [8] A. Simon and C. E. Clifford, The attenuation of neutrons by air ducts in shields, ORNL Report 1217, (March 1954).
- [9] A. T. Nelms, Graphs of the Compton energy-angle relationship and the Klein-Nishina formula from 10 Kev to 500 Mev, NBS Circular 542, (Aug. 1953).



Fig. 1. View of experimental duct with overhead shielding blocks removed. Detector at center is shown in typical position for measurement. Source is located in lead pig at upper right.

(TAN. $\alpha = 0.3$)

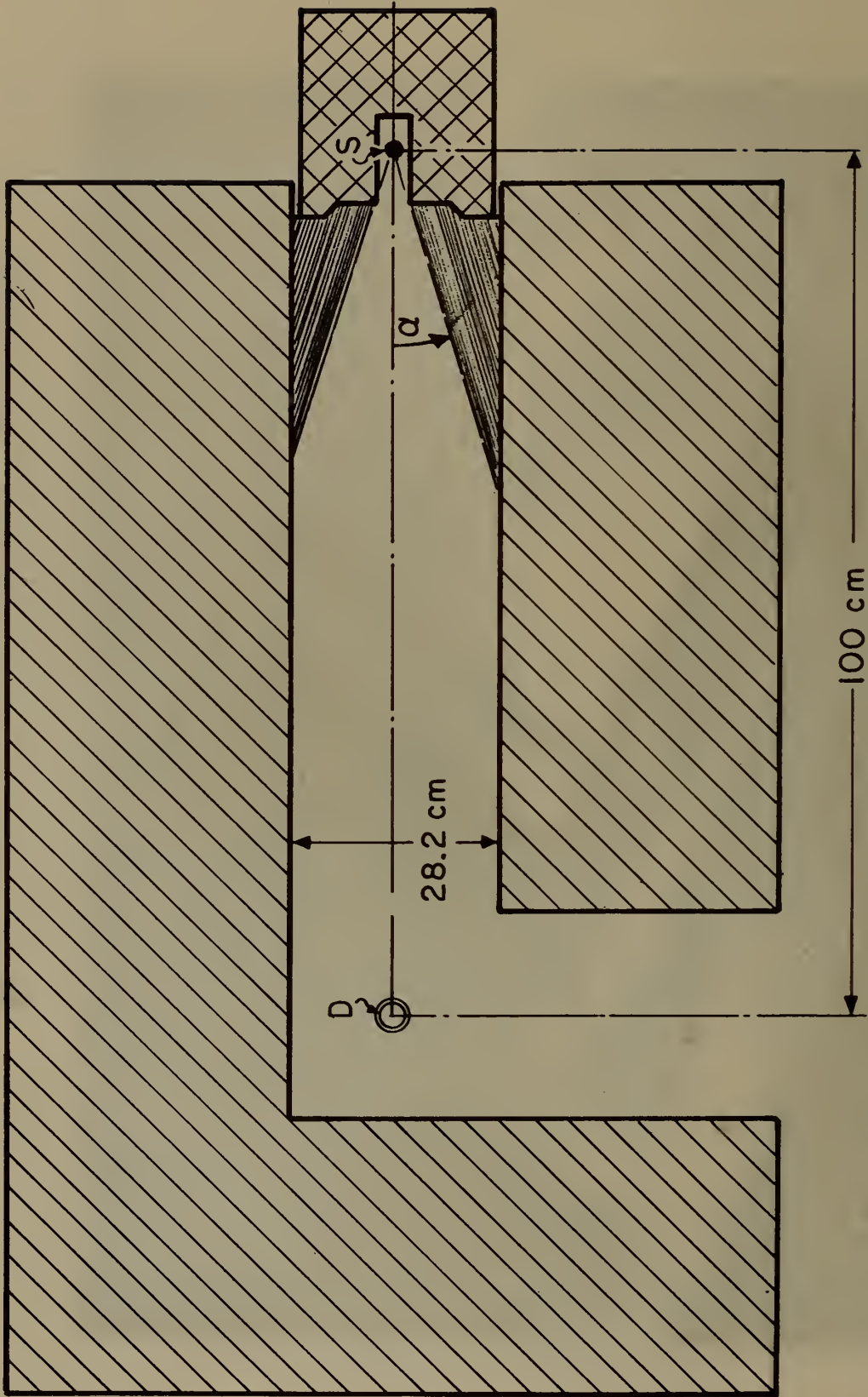


Fig. 2. Plan view of duct showing detector (D), source (S) and angle (α) of collimation.



Fig. 3. Detection equipment. At left is the 10 mr chamber mounted in aluminum holder. Two 200 mr pocket ionization chambers are also shown, one wrapped with tin for tests of energy response. The chambers were read on the Victoreen minimeter.

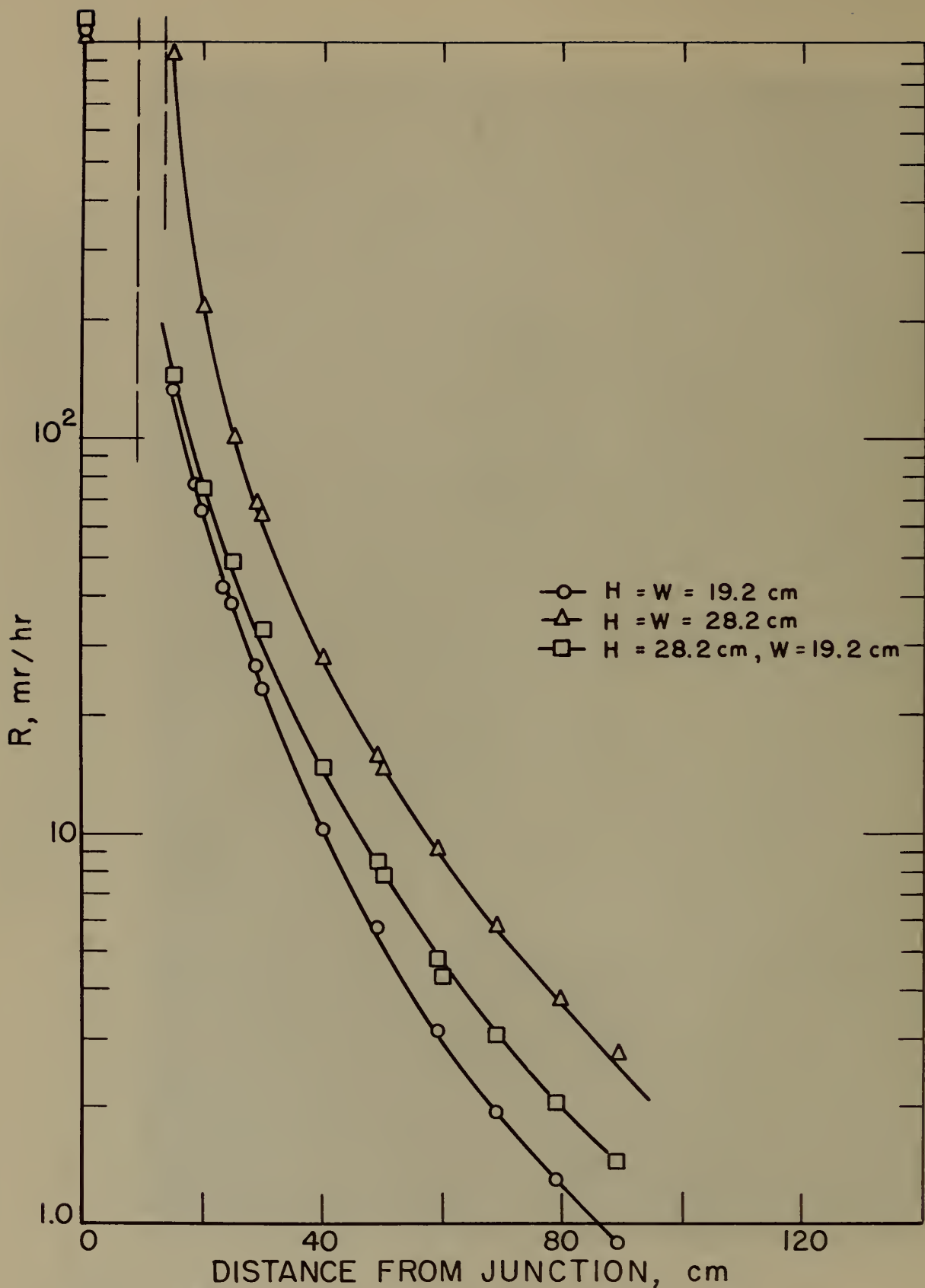


Fig. 4. Measured dose rates vs distance from the center of the junction. Results are shown for three ducts of different sizes.

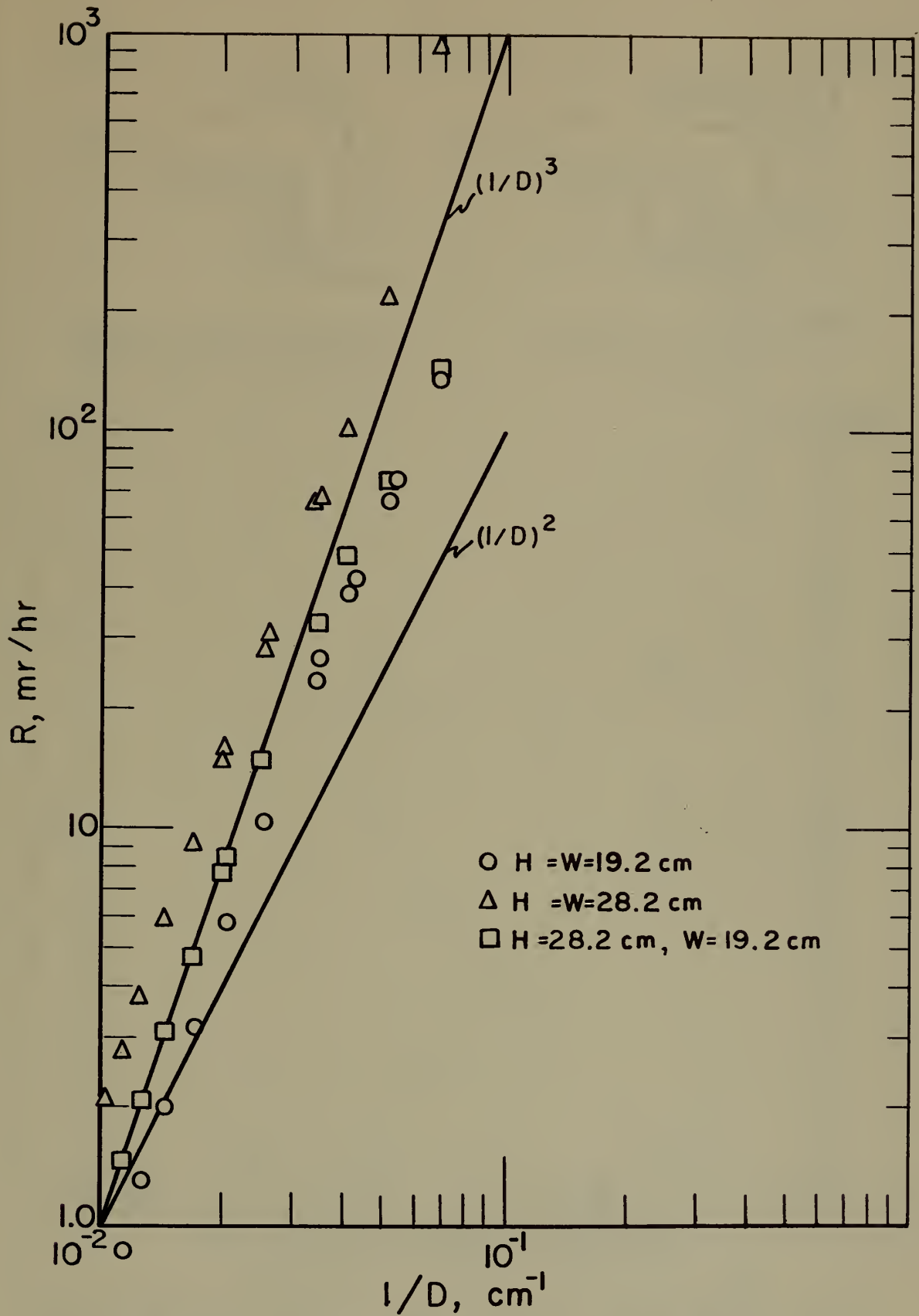


Fig. 5. Measured dose rates vs reciprocal distance for three different sized ducts.

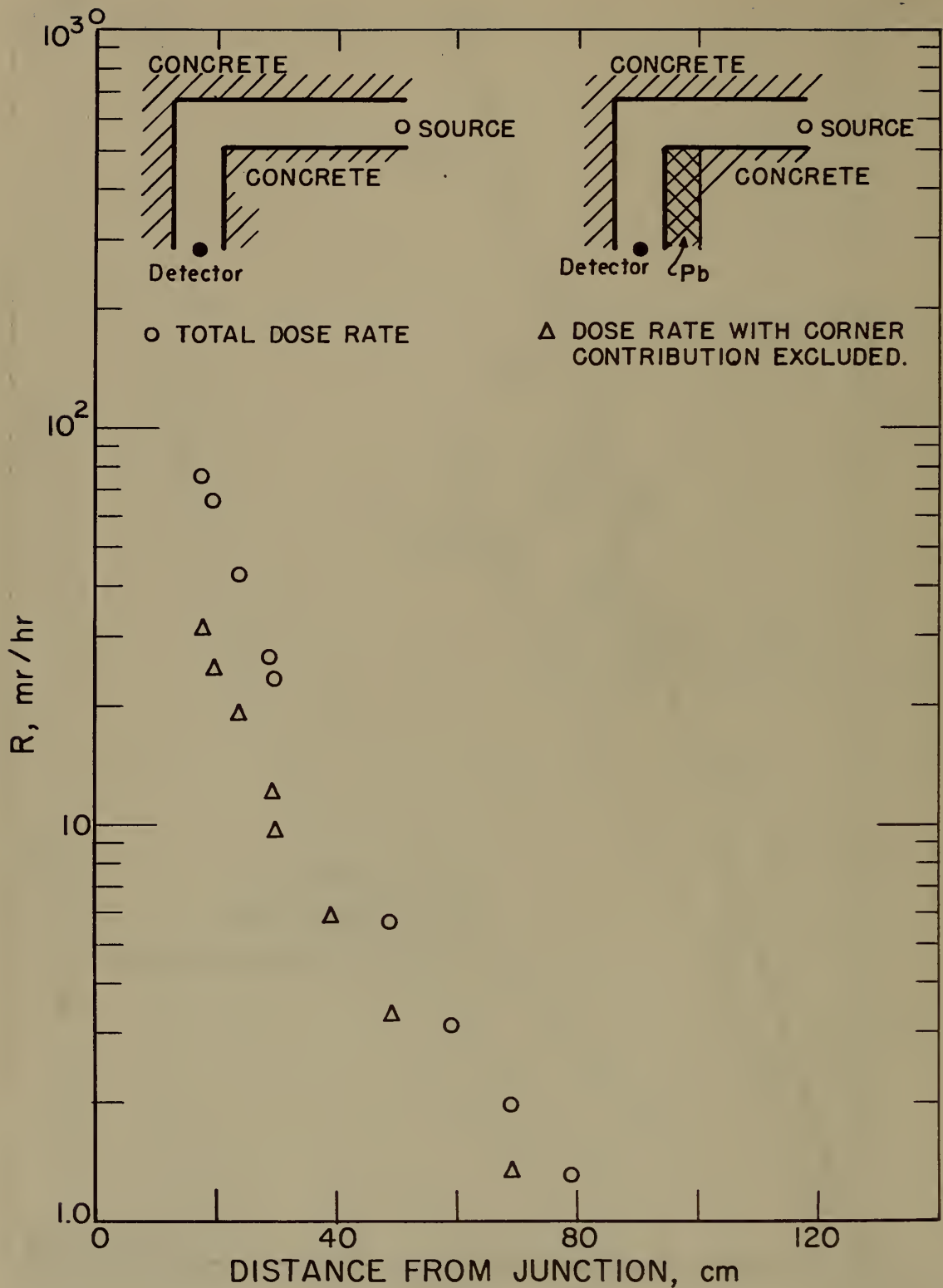


Fig. 6. Measured dose rate vs distance showing the difference in dose rates when the concrete corner is replaced by lead. Data were taken for a square duct with $H = W = 19.2$ cm.

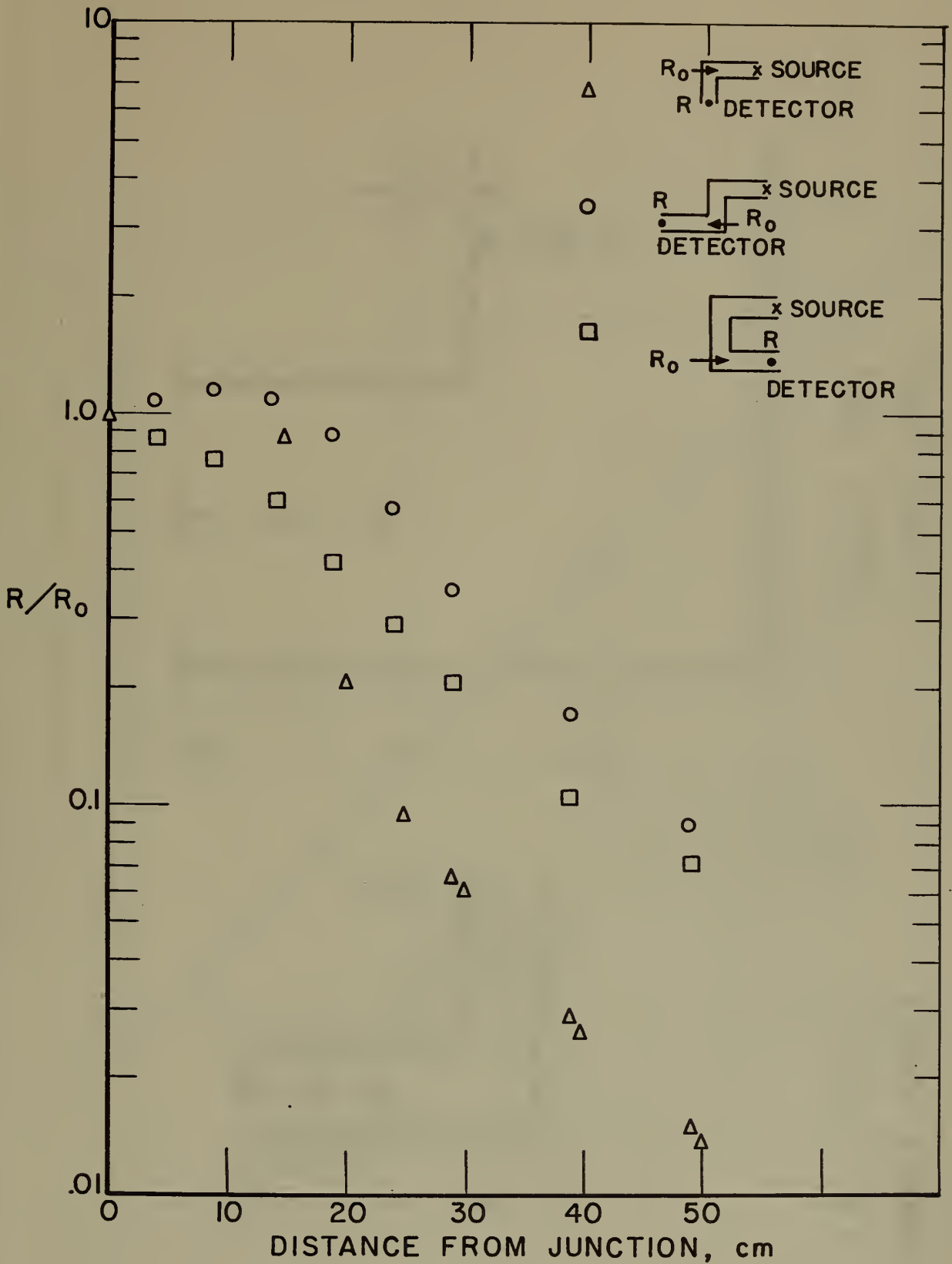
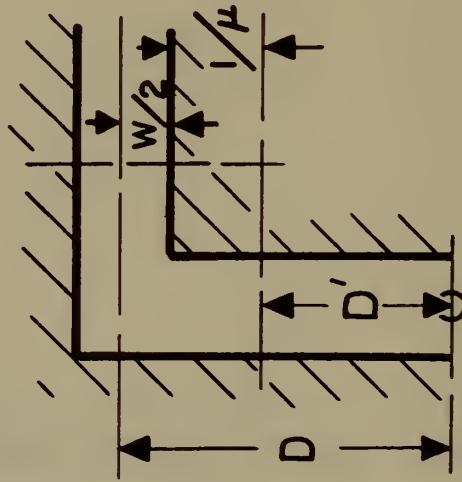


Fig. 7. Dose rate ratios vs distance after one and two right angle bends.

SMALL DUCT

($W \sim 1/\mu$)



LARGE DUCT

($W \gg 1/\mu$)

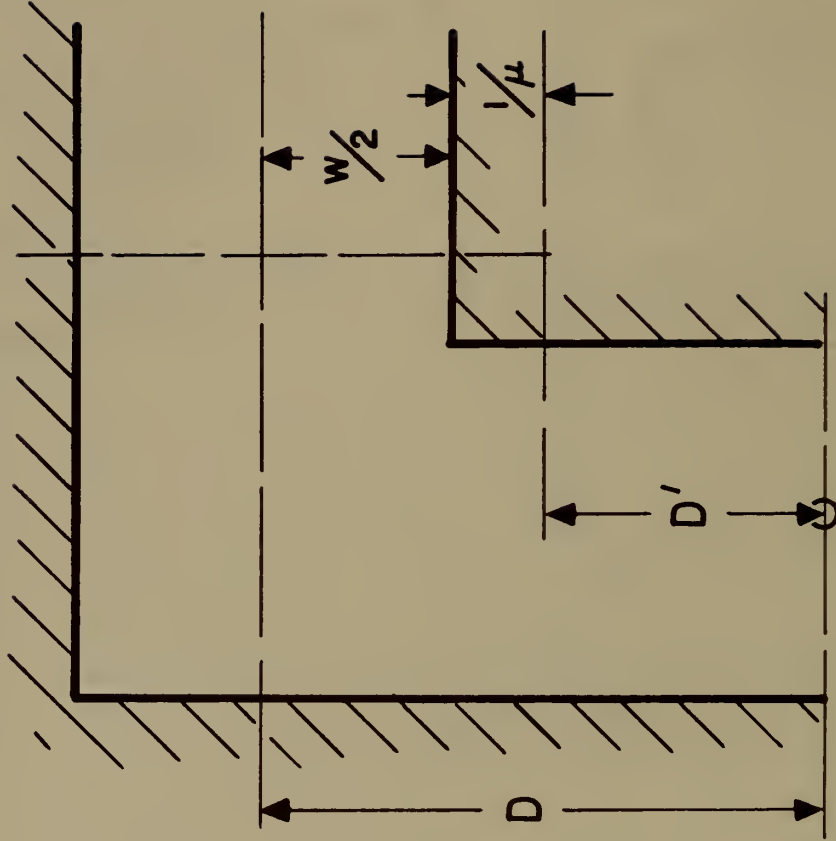


Fig. 8. Definition of distance D' for small and large ducts

$D' = D - \frac{W}{2} - 1/\mu$, where $1/\mu$ is the mean free path in the surrounding medium.

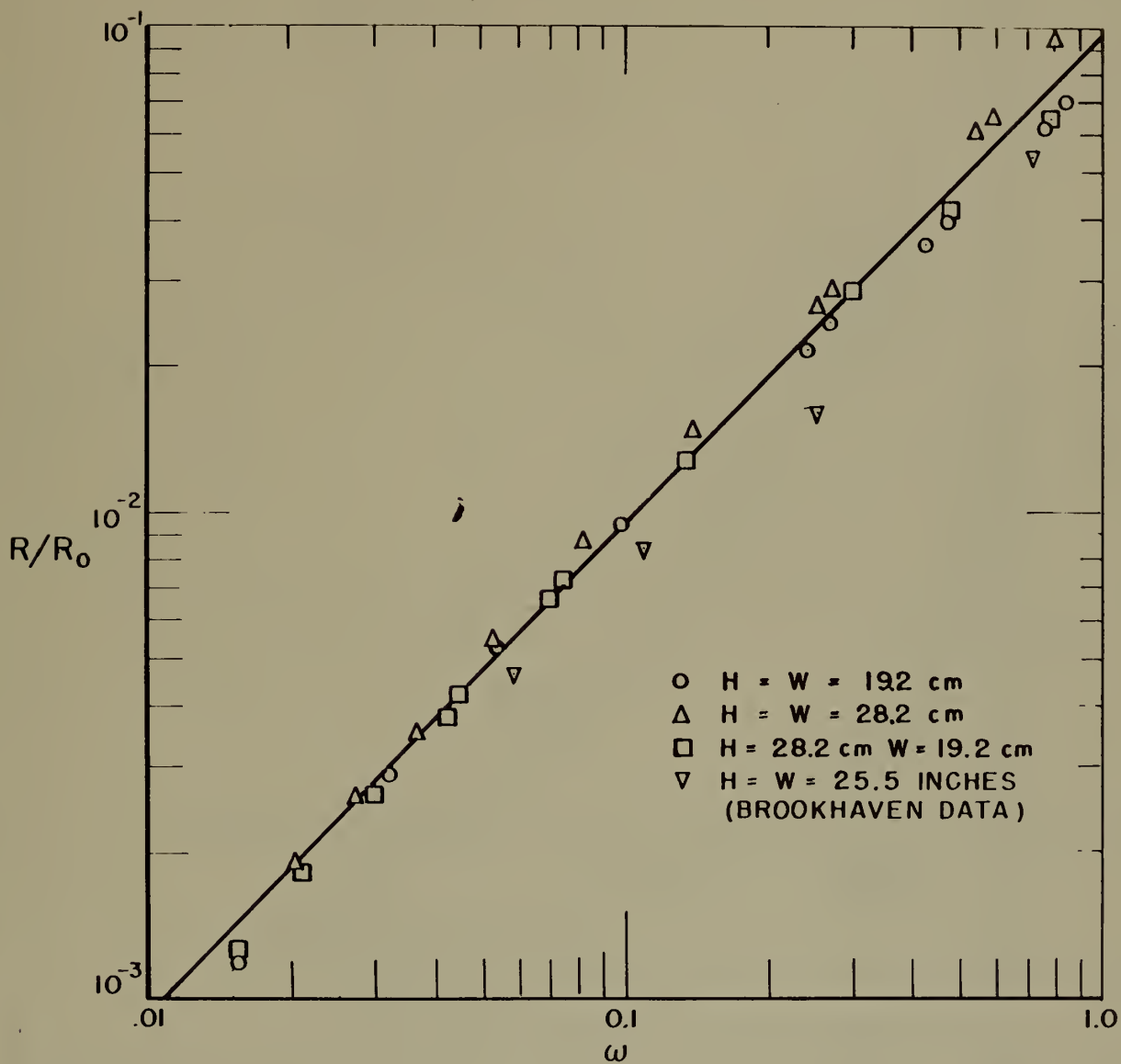


Fig. 9. Dose rate ratios vs solid angle fraction after one right angle bend.

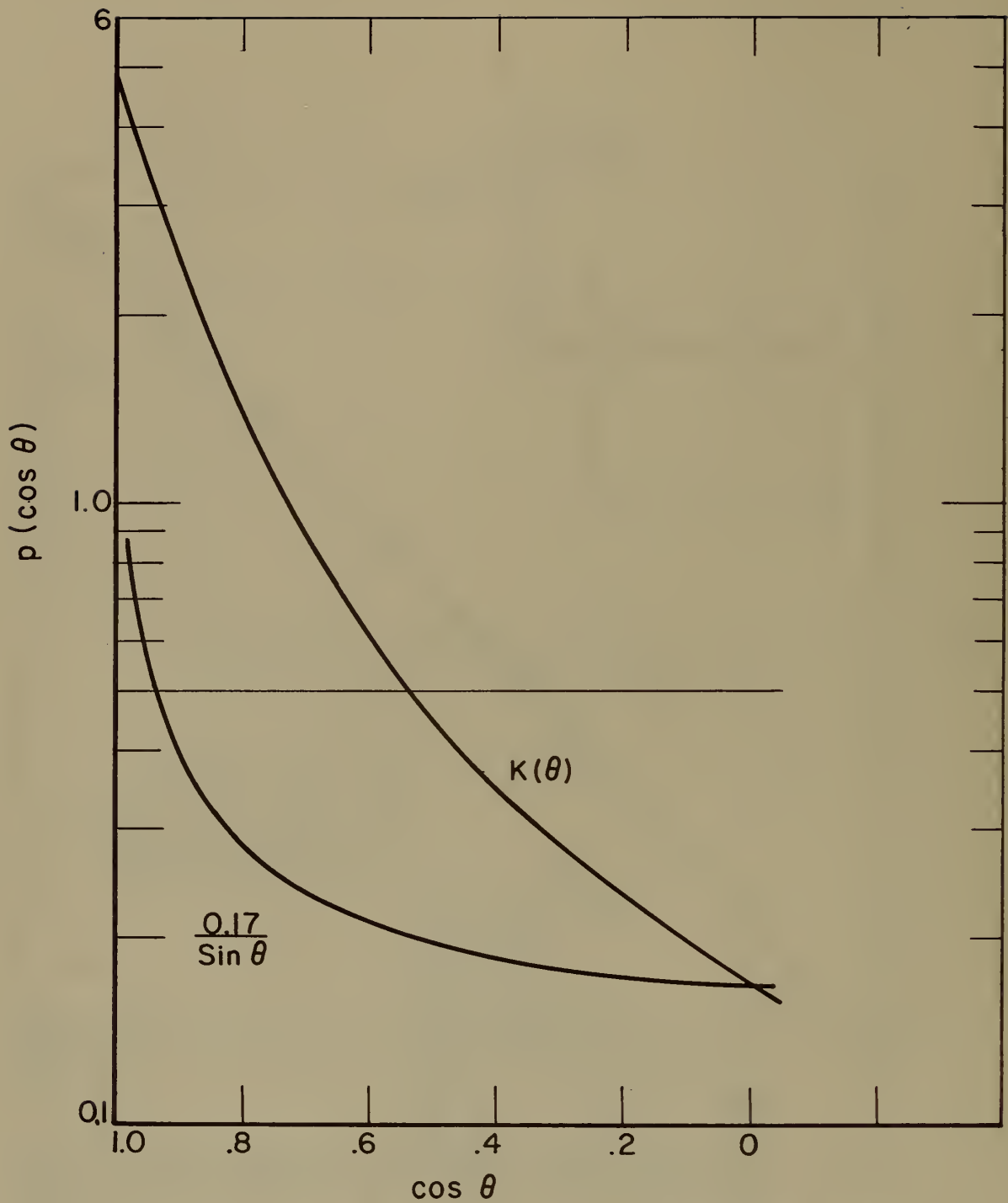


Fig. 10. Angular distributions of scattered energy from a beam of radiation. The horizontal line refers to an isotropic distribution, $K(\theta)$ is obtained from the Klein-Nishina formula for Cobalt-60 radiation, and the third curve is a normalized inverse sine distribution.

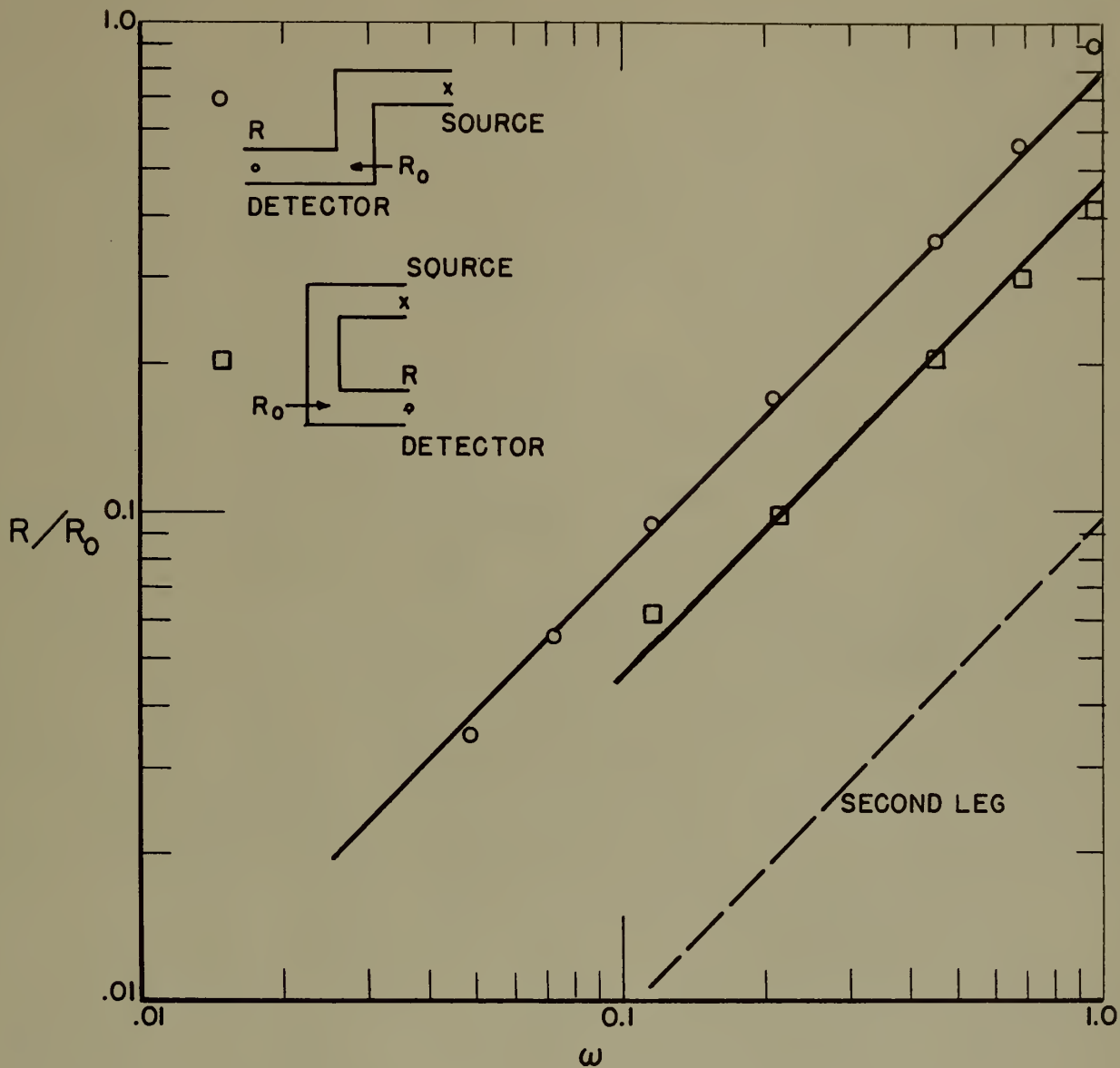


Fig. 11. Dose rate ratios vs solid angle fraction after two right angle bends. The dashed curve indicates the behavior in the second leg (after one right angle bend).

